Mesoporous Materials

DOI: 10.1002/ange.201308625

Ultralight Mesoporous Magnetic Frameworks by Interfacial Assembly of Prussian Blue Nanocubes**

Biao Kong, Jing Tang, Zhangxiong Wu, Jing Wei, Hao Wu, Yongcheng Wang, Gengfeng Zheng, and Dongyuan Zhao**

Abstract: *A facile approach for the synthesis of ultralight iron oxide hierarchical structures with tailorable macro- and mesoporosity is reported. This method entails the growth of porous Prussian blue (PB) single crystals on the surface of a polyurethane sponge, followed by in situ thermal conversion of PB crystals into three-dimensional mesoporous iron oxide (3DMI) architectures. Compared to previously reported ultralight materials, the 3DMI architectures possess hierarchical macro- and mesoporous frameworks with multiple advantageous features, including high surface area (ca. 117 $m^2 g^{-1}$) and ultralow density (6–11 $mg cm^{-3}$). Furthermore, they can be synthesized on a kilogram scale. More importantly, these 3DMI structures exhibit superparamagnetism and tunable hydrophilicity/hydrophobicity, thus allowing for efficient multiphase interfacial adsorption and fast multiphase catalysis.*

Three-dimensional (3D) porous materials with ultralow density are a research hotspot, owing to their high surface-to-volume ratio, easily accessible pore structures,[1] and tailorable surface functionalities for applications that include storage, separation, catalysis, drug delivery, and tissue engineering.[2] Silica-, carbon-, and metal-based materials, in the form of aerogels, sponges, networks, and microlattices,[3] contribute to almost all of the 3D porous materials for which densities below 10 $mg cm^{-3}$ have been reported. For instance, an ultralight carbon aerogel with a density of 0.16 $mg cm^{-3}$ was prepared by freeze-drying of an aqueous solution of carbon nanotubes and graphene oxide sheets.[3b] Very recently, an ultralight magnetic Fe_2O_3/carbon foam was synthesized on a centimeter scale by pyrolyzing commercial polyurethane (PU) sponge that had been grafted with metal acrylate; this foam was found to be very efficient in the absorption of oil from polluted water.[3c] Nonetheless, the obtained ultralight materials either lack organized mesoscale structures or are inherited from templates that are based on complex top-down methods, which limits the development of hierarchical structures and the design and control of mesostructure-based host–guest interfaces and leads to an increase in fabrication costs.

Whereas large pores and voids generally exist in ultralight materials, mesoporous materials represent another large category of unique structures with pore sizes between 2 and 50 nm.[4] These pores are typically produced by an organic–inorganic assembly of precursors and template molecules, which is followed by template removal to obtain organized pore structures. Combinations of mesoporous materials with large pores, such as sponges and polystyrene sphere assemblies,[5] have been used for preparing a variety of hierarchically porous structures, but none of these studies have demonstrated the synthesis of ultralight materials with densities that are comparable to those of aerogels or foams. More critically, the transition metal oxide precursors typically undergo fast hydrolysis or condensation reactions so that they can only weakly interact with template molecules,[6] which renders the synthesis of metal oxides (such as iron oxide) mesostructures a substantial challenge. To date, a scalable synthesis of ultralight 3D transition metal oxides with hierarchical macro- and mesoporous structures has not been described.

Herein, an interface-mediated growth of 3DMI frameworks is described that was achieved by the controlled hydrolysis and assembly of molecular precursors on the solution–substrate interface without structure-directing surfactants, followed by an interface-constrained thermal pyrolysis of the porous coordination polymer network (PCPN) nanocrystals into the 3DMI frameworks with hierarchical macropores and mesopores (Figure 1). The compounds of the Prussian blue family are among the most well-known PCPNs,[7] with a typical chemical formula of $M_3[M'(CN)_6]_2 \cdot n H_2O$, and based on a cubic (α-Po) network topology, where the M and M′ ions are connected to the cyanide ions by linear M–CN–M′ linkages. PU sponges with inverse opal surfaces and different pore sizes (600–1250 μm; Figure 2a,d) were used as the growth substrates for the hydrolysis of $K_4[Fe(CN)_6]$ (for details, see the Supporting Information). After the synthesis, the color of the PU sponges changed from yellow to blue, suggesting that Prussian blue

[*] B. Kong,[+] J. Tang,[+] H. Wu, Y. Wang, Prof. G. Zheng, Prof. D. Zhao
Department of Chemistry
Laboratory of Advanced Materials
Shanghai Key Laboratory of Molecular Catalysis and Innovative Materials, Fudan University
Shanghai 200433 (P.R. China)
E-mail: gfzheng@fudan.edu.cn
dyzhao@fudan.edu.cn
B. Kong,[+] Z. Wu, J. Wei
Department of Chemical Engineering, Monash University
Wellington Road, Clayton, VIC 3800 (Australia)
[+] These authors contributed equally to this work.

[**] This work was supported by the National Key Basic Research Program of China (2013CB934104, 2012CB224805), the NSF of China (20890123, 21322311, and 21071033), the Shanghai Leading Academic Discipline Project (B108), the Science and Technology Commission of Shanghai Municipality (08DZ2270500), the Program for New Century Excellent Talents in University (NCET-10-0357), and the Program for Professor of Special Appointment (Eastern Scholar) at Shanghai Institutions of Higher Learning.

Supporting information for this article is available on the WWW under http://dx.doi.org/10.1002/anie.201308625.

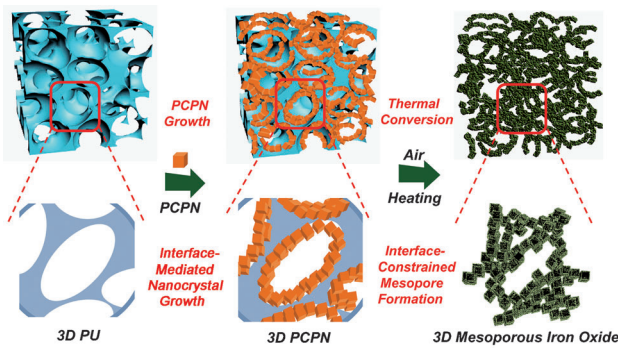

Figure 1. Growth of ultralight 3DMI architectures. Three-dimensional PU is used as the scaffold for the interfacial growth of PB–PCPN nanocubes. Subsequent thermal treatment removes the PU scaffold and converts the PB nanocubes into iron oxides. The obtained 3DMI material replicates the morphology of the initial scaffold, while forming mesoporous structures inside the nanocubes at the same time.

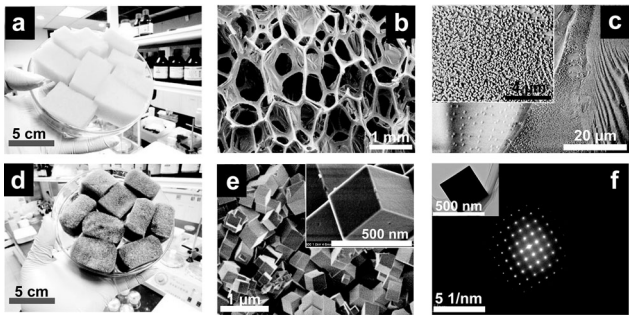

Figure 2. a, d) Photographs of the PU scaffold before (a) and after (d) interfacial growth. b) SEM image of soft PU foam scaffolds. c) SEM images of the PCPN nanocrystals with the nanocube morphology grown on the PU scaffold. Inset: Magnified SEM image of a single frame of the PU scaffolds. e) PCPN nanocrystals with high density on the scaffolds. Inset: SEM image of a single PCPN crystal. f) TEM image and corresponding SAED pattern of one PCPN nanocrystal.

nanocubes had grown (Figure 2b and Figure S1). Scanning electron microscopy (SEM) revealed that the PU surfaces are covered by nanocubes with sharp edges and a uniform size of approximately 300 nm (Figure 2c,e). High-resolution transmission electron microscopy (HRTEM) images show that all Prussian blue nanocubes are solid and of a uniform size (Figure 2f and Figure S2). The selected area electron diffraction (SAED) pattern of a single nanocube along the $< 001 >$ zone axis exhibits ordered diffraction spots, which indicates that the Prussian blue nanocubes are of a single-crystalline nature (Figure 2f).[8] The crystallographic structure of the Prussian blue nanocubes was further confirmed by powder X-ray diffraction (XRD); all of the diffraction peaks could be assigned to the face-centered-cubic $Fe_4[Fe(CN)_6]_3$ structure (Figure S3),[9] which suggests that the material is of high purity. Furthermore, the PU foams that are loaded with Prussian blue nanocubes could preserve their high flexibility. The Prussian blue nanocubes are hardly flexible owing to their face-centered-cubic $Fe_4[Fe(CN)_6]_3$ crystal structure. After they had been grown on the polyurethane surface, the flexibility of the Prussian blue polyurethane nanocubes was much greater. Two distinctive stages were observed during stress tests ($\varepsilon_{max} = 60\,\%$), including a quasi-linear elastic region at $\varepsilon < 50\,\%$, which is followed by a densification region (Figure S4). This process is highly reversible and reproducible for more than 30 cycles.

The as-prepared Prussian blue nanocubes were subsequently converted into Fe_2O_3 nanocubes by pyrolysis in air. The resulting product exhibited a similar framework, but its pore size was smaller than that of the initial PU sponge scaffold, which indicates that a replication and contraction process of the PU macroporous frameworks has occurred. The macropores are approximately 250 μm large (Figure 3a and Figure S5), and the struts of the 3D framework consist of layers of packed nanocubes (Figure 3b and Figure S6). The layer thickness is approximately 1.2 μm, which corresponds to approximately three nanocube layers. These nanocubes have a mesoporous structure over the entire cube with a polycrystalline nature (Figure 3c,d). HRTEM images reveal that the nanocubes are assembled by fully crystallized iron oxide nanoparticles with uniform sizes of < 10 nm (Figure 3e,f).[10]

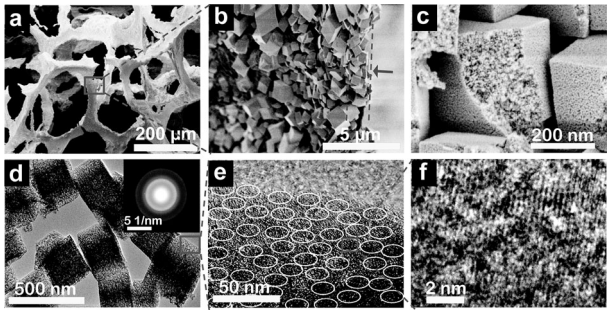

Figure 3. a–c) SEM images of 3DMI architectures. d) TEM image and corresponding SAED pattern (inset) of the 3D mesoporous superparamagnetic architectures. e) TEM image of a corner of the superparamagnetic mesoporous nanocubes. The white circles indicate the component units of crystallized iron oxide nanoparticles after pyrolysis in air. f) HRTEM image of a crystallized iron oxide nanoparticle in superparamagnetic mesoporous nanocubes.

The N_2 sorption isotherms of the 3DMI frameworks that were obtained after calcination at 350–450 °C show type IV curves with surface areas of approximately 93, 105, and 117 $m^2 g^{-1}$ (Figure 4a), and mean pore sizes of approximately 12.7, 14.1, and 18.3 nm, respectively (Figure 4b). The wide-angle XRD pattern reveals that the PCPN-derived 3DMI nanocubes are mainly composed of a γ-Fe_2O_3 phase (Figure S7a).[11] The diffraction peaks of γ-Fe_2O_3 gradually increase in intensity (from 350 to 450 °C) without phase changes (Figure S8). X-ray photoelectron spectroscopy (XPS) of 3DMI nanocubes revealed two main peaks at approximately 725 and 710 eV, which may be associated with the Fe $2p_{1/2}$ and $2p_{2/3}$ of γ-Fe_2O_3 (Figure S7b,c), respectively.[12] The obtained 3DMI framework exhibits attractive superparamagnetic properties as it benefits from the controlled crystalline phases and grain sizes. The magnetization curves of 3DMI frameworks show almost no hysteresis loops and only very

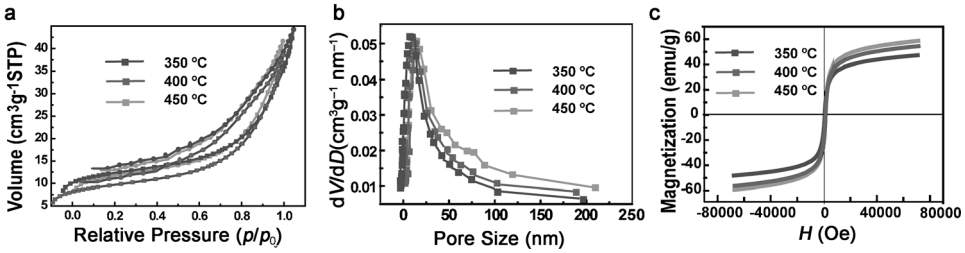

Figure 4. a) Nitrogen sorption isotherms. b) Pore size distribution. c) Magnetization curve for the 3D mesoporous structure.

small remnant magnetization (M_r) and coercive force (H_c) at room temperature, suggesting a superparamagnetic or quasi-superparamagnetic behavior (Figure 4i).[13]

The surface wettability of the 3DMI frameworks can be easily tuned from highly hydrophilic to highly hydrophobic by surface functionalization.[14] Water droplets that were deposited on the as-grown 3DMI frameworks quickly spread out on the surface with a low contact angle (<1°; Figure S7d), indicating the hydrophilic nature of the pristine 3DMI structures. After coating with phenolic resins (resols) and subsequent thermal treatment (for details, see the Supporting Information), the water contact angles ranged from 83.6° to 117.5° with an increase in the resol deposition time, suggesting a hydrophobic surface (Figure S7e,f). Furthermore, the 3DMI frameworks exhibited high thermal stability even when they were exposed to an alcohol flame (400–600 °C, depending on the part of the flame), as both the morphology and the nanostructure were well retained (Figures S7g, S9, S10).

Aside from the 3D hierarchical porosity, superparamagnetism and tunable surface hydrophobicity, the 3DMI frameworks offer remarkable ultralow density and convenient tailorability, which may be attributed to abundant pores, hierarchical stacking, and the non-rigid connection of the mesoporous nanocube building blocks. The density was measured to be as low as approximately 6 mg cm^{-3}, which makes this framework one of the lightest metal oxide materials with a density that is comparable to those of ultralight silica-, carbon-, and metal-based structures.[3a,b] For instance, a 3DMI piece of approximately 1.46 g and 240 cm^3 can be placed on top of an oleander flower (Figure 5a,b). Furthermore, the bulk 3DMI frameworks can be conveniently tailored into desired shapes, such as ultrathin films, cylinders, cubes, hexagons, or triangular prisms (Figure 5c,e; see also Figure S11) or packed as functional columns for filtration, adsorption, and catalysis (Figure 5d and Figure S11d). The 3D structures were well preserved without structure cracking.

More importantly, this synthetic method for 3DMI frameworks is scalable for mass production and possible practical applications. For instance, by using multiple (ca. 50) PU foams, each with a volume of 4500 cm^3, which were incubated with a Prussian blue precursor solution in a 5.5 L reaction container, approximately 1.26 kg of 3DMI frameworks were produced (Figure 5f,g; see also Figures S12, S13). Moreover, this method can be extended to a large variety of substrates, including carbon fibers, silkworm, wool, and glass fibers (Figure S14). Therefore, this approach is highly flexible and may be used for the synthesis of other 3DMI structures for various applications.

Possible applications of the 3DMI framework arise from its strong magnetic properties (Figure 5h), hierarchical porosity, high surface area, and tunable surface functionalities. The large pore sizes can expedite molecule transport,[15,16] whereas the mesopores provide large adsorption sites for target molecules. The outstanding magnetic and adsorption properties of the 3DMI structures were first demonstrated for the removal of heavy metal ions, such as As^{III}, from contaminated water. The As^{III} ions can be selectively adsorbed onto the iron(III) oxide particles by ligand exchange in the coordination spheres of the structurally defining Fe atoms (Table S1).[17] The 3DMI materials could rapidly remove 95 wt% of the As^{III} ions (δ = 5 ppm in an aqueous solution) within 20 min (Figure 5i) and are thus much more efficient than magnetic Fe_2O_3 nanoparticles with diameters of 8 or 170 nm. The removal percentage of the As^{III} ions was improved by 168% and

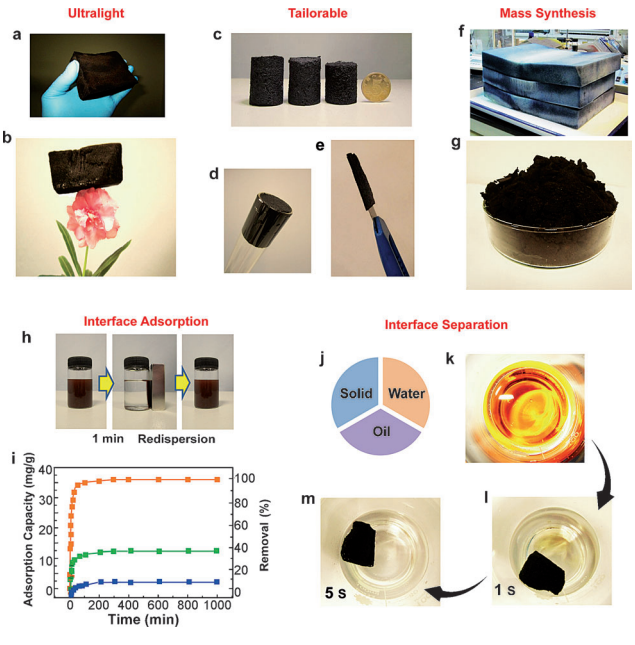

Figure 5. a) Bulk ultralight 3DMI architecture. b) A 3DMI architecture with a volume of 240 cm^3 can be placed on top of an oleander flower. c) 3DMI materials can be tailored into a cylindrical shape. d) Filtration column filled with 3DMI material of cylindrical shape. e) An ultrathin 3DMI sheet on a sharp blade. f,g) Photographs of Prussian blue coated polyurethane sponge and the 3DMI powder. h) Collection of the 3DMI powder with a magnet. i) Time-dependent capture of As^{III} ions by the 3DMI material with an initial arsenic concentration of δ = 5 ppm (——), compared to the uptake by iron oxide NPs with diameters of 8 (——) and 170 nm (——). j–m) Uptake of an organic liquid by the hydrophobic 3DMI architecture in a solid–water–oil triphasic system. A layer of Sudan III-stained gasoline was completely absorbed by a monolith of the hydrophobic 3DMI architecture in five seconds.

1315%, compared to their removal by the magnetic nanoparticles with diameters of 8 and 170 nm, respectively.

The excellent adsorption performance of the 3DMI frameworks was further shown by oil–water separation. A small piece (ca. 2.83 cm^3) of resol-coated 3DMI material can complete adsorb Sudan III-stained gasoline from water (Figure 5j–l).[18] This oil adsorption/removal has been interrogated for various petroleum products, including gasoline, diesel, and pump oil. The resol-coated 3DMI materials exhibited a high adsorption capacity that amounts to more than 150 times their own weight, which is higher than for other reported porous materials, such as Fe/C (ca. 10 times), PU (ca. 20 times), cellulose aerogels (ca. 40 times), graphene sponges (ca. 80 times), Fe_2O_3/C foam (ca. 100 times), and graphene/carbon nanotube sponges (ca. 130 times), and comparable to that of carbon nanotube sponges (ca. 180 times).[3c]

Furthermore, the resol-coated 3DMI frameworks were used as a nanoreactor for multiphase catalysis. The formation of benzaldehyde from natural cinnamaldehyde by a retro-aldol condensation is used as a representative water–oil biphasic reaction, which usually requires phase transfer reagents and co-solvents.[19] Adding resol-coated 3DMI catalysts led to a short reaction time (< 20 h), excellent selectivity (ca. 99%) and high conversion (ca. 93%; Figure S15–S17, Table S2). These results are comparable to those that were obtained with phase transfer reagents or co-solvent, and substantially higher (ca. 447%) than for a reaction that is run in the absence of resol-coated 3D MIs. This high yield is attributed to the tunable hydrophilic/hydrophobic surface of the 3DMI frameworks, which may thus accommodate both hydrophilic Na_2CO_3 and hydrophobic cinnamaldehyde and enable efficient molecule transfer across the oil–water interface.[19b,20] The catalysts can be magnetically recovered and were reused more than 15 times without a significant drop in conversion.

The successful synthesis of the ultralight mesoporous 3DMI frameworks is attributed to the interface-mediated crystal growth and pyrolysis. First, the PU sponge surface bears many carbamate groups (NH–COO) on its main chains and can efficiently adsorb the hydrolysis products of the $K_4[Fe(CN)_6]$ precursor (Figure 6a). The hydrolysis and condensation of $K_4[Fe(CN)_6]$ rapidly proceeded on the PU–solution interface, with each nitrogen terminus in a ferrocyanide complex featuring an octahedral geometry, and formed a Fe^{2+}–CN–Fe^{3+} linkage layer by layer.[21] Increasing the growth time led to the accumulation of Prussian blue nanocubes on the PU surface. Afterwards, the single-crystalline Prussian blue nanocubes were decomposed by thermal treatment (Figure 6b,c), during which gaseous products (e.g., CO_2) were released, which created a shrinking force for the nanocubes. Nonetheless, as the Fe–O bonds on the surface are tightly bound to the adjacent nanocubes and the substrate underneath, this shrinking force does not result in morphology deformation of the nanocube assembly. Instead, this surface-constrained pyrolysis can well retain the shapes and connections of the 3DMI nanocubes, while forming mesopores inside the nanocubes. Therefore, the obtained 3DMI frameworks preserve the morphology of the Prussian blue

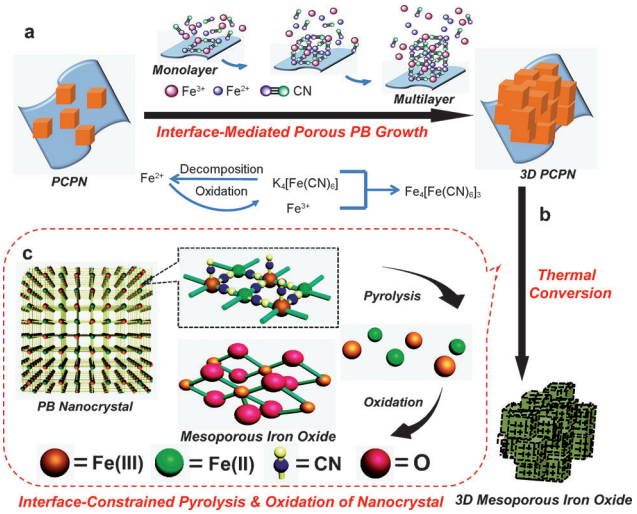

Figure 6. Proposed mechanism of formation. a) Interface-induced growth and self-assembly mechanism and reaction process for the preparation of three-dimensional Prussian blue coordination polymer networks on universal 3D frames. $K_4[Fe(CN)_6]$ undergoes hydrolysis and condensation on the interface of the three-dimensional PU foam and nucleates to form a linear Fe^{2+}–CN–Fe^{3+} linkage layer by layer. Increasing the growth time leads to the accumulation of cubic Prussian blue crystals on the PU surface. b,c) Formation mechanism for 3D PCPNs and corresponding mesoporous iron oxide obtained by thermal conversion. Interfacial growth of the three-dimensional PB nanocrystal was achieved by a scalable solution-phase synthesis that is based on decomposition and oxidation of the precursors on the 3D template interface.

nanocubes and form continuous layers, which replicate the original PU sponges and inherit the macropores. Furthermore, the 3DMI frameworks are composed of interconnected γ-Fe_2O_3 nanocrystals with uniform sizes of approximately 10 nm, which are slightly smaller than those calculated according to the Scherrer Equation, thus confirming the preferred orientation of the Fe_2O_3 nanocrystals.

Compared to the widely used sol–gel and evaporation-induced self-assembly (EISA) methods for creating mesoporous structures,[22] this method utilizes surface interactions for crystal growth and subsequent mesopore formation. This approach has not been applied to transition metal oxides in the absence of template molecules. More importantly, this approach can be conveniently scaled up at low cost, and the obtained products inherit the tailorability of the three-dimensional PU foam templates, which can be easily handled, cut, and assembled without affecting their physical and chemical properties. Combining the ultralight properties, large surface area, and suitable mesopore sizes, abundant surface chemistry allows for using the 3DMI materials for a number of applications, including filtration, adsorption, and multiphase catalysis. For filtration and adsorption, the large pore sizes can expedite the transport of solution, whereas the mesopores provide large adsorption sites for impurities, such as heavy metal ions and oil molecules. For multiphase catalysis, the addition of the 3DMI materials allows for efficient molecule transfer between oil and water phases, which leads to an increased conversion while obviating the need for additional phase transfer reagents and co-solvents.

In summary, we have developed a facile synthesis of ultralight 3DMI frameworks by surface-induced crystal growth of Prussian blue nanocubes and subsequent surface-constrained mesopore formation. The 3DMI frameworks have a high surface area (ca. 117 $m^2 g^{-1}$) and a hierarchical macro- and mesoporous structure, with bimodal mean pore sizes of 250 μm and 18 nm. The density of the 3DMI framework is as low as approximately 6 $mg cm^{-3}$, which is comparable to that of ultralight silica-, carbon-, and metal-based structures. The developed method allowed for the synthesis of approximately 1.26 kg of tailorable 3DMI material. These ultralight 3DMI frameworks exhibit characteristics that include superparamagnetism, a tunable surface, as well as hydrophilicity and hydrophobicity, which allows for the adsorption of heavy metal ions and organic molecules and multiphase catalysis. Further developments of this surface-mediated crystal growth and mesopore formation can lead to many opportunities for synthesizing a variety of ultralight mesoporous transition metal oxides.

Received: October 3, 2013
Revised: December 7, 2013
Published online: February 12, 2014

Keywords: adsorption · catalysis · magnetic properties · mesoporous materials · ultralight materials

[1] a) B. Tian, J. Liu, T. Dvir, L. Jin, J. H. Tsui, Q. Qing, Z. Suo, R. Langer, D. S. Kohane, C. M. Lieber, *Nat. Mater.* **2012**, *11*, 986 – 994; b) R. T. Olsson, M. A. Samir, G. Salazar-Alvarez, L. Belova, V. Ström, L. A. Berglund, O. Ikkala, J. Nogues, U. W. Gedde, *Nat. Nanotechnol.* **2010**, *5*, 584 – 588.

[2] a) Y. Xu, Z. Lin, X. Huang, Y. Liu, Y. Huang, X. Duan, *ACS Nano* **2013**, *7*, 4042 – 4049; b) H. Wu, D. Kong, Z. Ruan, P.-C. Hsu, S. Wang, Z. Yu, T. J. Carney, L. Hu, S. Fan, Y. Cui, *Nat. Nanotechnol.* **2013**, *8*, 421 – 425.

[3] a) Y. Shao, J. Xiao, W. Wang, M. Engelhard, X. Chen, Z. Nie, M. Gu, L. V. Saraf, G. Exarhos, J.-G. Zhang, J. Liu, *Nano Lett.* **2013**, *13*, 3909 – 3914; b) H. Sun, Z. Xu, C. Gao, *Adv. Mater.* **2013**, *25*, 2554 – 2560; c) N. Chen, Q. Pan, *ACS Nano* **2013**, *7*, 6875 – 6883; d) T. Schaedler, A. Jacobsen, A. Torrents, A. Sorensen, J. Lian, J. Greer, L. Valdevit, W. Carter, *Science* **2011**, *334*, 962 – 965.

[4] B. Tian, X. Liu, B. Tu, C. Yu, J. Fan, L. Wang, S. Xie, G. D. Stucky, D. Zhao, *Nat. Mater.* **2003**, *2*, 159 – 163.

[5] a) Y. Deng, J. Wei, Z. Sun, D. Zhao, *Chem. Soc. Rev.* **2013**, *42*, 4054 – 4070; b) J. Wei, H. Wang, Y. Deng, Z. Sun, L. Shi, B. Tu, M. Luqman, D. Zhao, *J. Am. Chem. Soc.* **2011**, *133*, 20369 – 20377.

[6] W. Li, J. Yang, Z. Wu, J. Wang, B. Li, S. Feng, Y. Deng, F. Zhang, D. Zhao, *J. Am. Chem. Soc.* **2012**, *134*, 11864 – 11867.

[7] S. Ferlay, T. Mallah, R. Ouahes, P. Veillet, M. Verdaguer, *Nature* **1995**, *378*, 701 – 703.

[8] a) J. Keggin, F. Miles, *Nature* **1936**, *137*, 577 – 578; b) L. Zhang, H. B. Wu, S. Madhavi, H. H. Hng, X. W. Lou, *J. Am. Chem. Soc.* **2012**, *134*, 17388 – 17391.

[9] C. Wang, L. Zhang, Z. Guo, J. Xu, H. Wang, H. Shi, K. Zhai, X. Zhuo, *Electroanalysis* **2010**, *22*, 1867 – 1872.

[10] Y. Chao, P. P. Karmali, R. Mukthavaram, S. Kesari, V. L. Kouznetsova, I. F. Tsigelny, D. Simberg, *ACS Nano* **2013**, *7*, 4289 – 4298.

[11] C. Garcia, Y. Zhang, F. DiSalvo, U. Wiesner, *Angew. Chem.* **2003**, *115*, 1564 – 1568; *Angew. Chem. Int. Ed.* **2003**, *42*, 1526 – 1530.

[12] X. Dong, H. Chen, W. Zhao, X. Li, J. Shi, *Chem. Mater.* **2007**, *19*, 3484 – 3490.

[13] Z. G. Estephan, H. H. Hariri, J. B. Schlenoff, *Langmuir* **2013**, *29*, 2572 – 2579.

[14] Y. Meng, D. Gu, F. Zhang, Y. Shi, H. Yang, Z. Li, C. Yu, B. Tu, D. Zhao, *Angew. Chem.* **2005**, *117*, 7215 – 7221; *Angew. Chem. Int. Ed.* **2005**, *44*, 7053 – 7059.

[15] A. H. Lu, W. Schmidt, N. Matoussevitch, H. Bönnemann, B. Spliethoff, B. Tesche, E. Bill, W. Kiefer, F. Schüth, *Angew. Chem.* **2004**, *116*, 4403 – 4406; *Angew. Chem. Int. Ed.* **2004**, *43*, 4303 – 4306.

[16] A. H. Lu, J. J. Nitz, M. Comotti, C. Weidenthaler, K. Schlichte, C. W. Lehmann, O. Terasaki, F. Schuth, *J. Am. Chem. Soc.* **2010**, *132*, 14152 – 14162.

[17] a) Z. Wu, W. Li, P. A. Webley, D. Zhao, *Adv. Mater.* **2012**, *24*, 485 – 491; b) L. Cumbal, A. Sengupta, *Environ. Sci. Technol.* **2005**, *39*, 6508 – 6515.

[18] Z. Y. Wu, C. Li, H. W. Liang, J. F. Chen, S. H. Yu, *Angew. Chem.* **2013**, *125*, 2997 – 3001; *Angew. Chem. Int. Ed.* **2013**, *52*, 2925 – 2929.

[19] a) D. R. Rolison, *Science* **2003**, *299*, 1698 – 1701; b) X. Zuwei, Z. Ning, S. Yu, L. Kunlan, *Science* **2001**, *292*, 1139 – 1141.

[20] a) Y. Nitta, Y. Hiramatsu, T. Imanaka, *J. Catal.* **1990**, *126*, 235 – 245; b) F. Berthiol, H. Doucet, M. Santelli, *Catal. Lett.* **2005**, *102*, 281 – 284.

[21] a) H. Tokoro, K. Nakagawa, K. Imoto, F. Hakoe, S.-i. Ohkoshi, *Chem. Mater.* **2012**, *24*, 1324 – 1330; b) N. D. Petkovich, A. Stein, *Chem. Soc. Rev.* **2013**, *42*, 3721 – 3739.

[22] a) Y. Wan, D. Zhao, *Chem. Rev.* **2007**, *107*, 2821 – 2860; b) Y. Fang, Y. Lv, R. Che, H. Wu, X. Zhang, D. Gu, G. Zheng, D. Zhao, *J. Am. Chem. Soc.* **2013**, *135*, 1524 – 1530.

